Modifying last layer in polyelectrolyte multilayer coatings for capillary electrophoresis of proteins

Sébastien Roca, Laurent Leclercq, Philippe Gonzalez, Laura Dhellemmes, Laurent Boiteau, Gaulthier Rydzek, Hervé Cottet

Modifying last layer in polyelectrolyte multilayer coatings for capillary electrophoresis of proteins

Sébastien Roca[1], Laurent Leclercq[1*], Philippe Gonzalez[1], Laura Dhellemmes[1], Laurent Boiteau[1], Gaulthier Rydzek[2], Hervé Cottet[1*]

[1] IBMM, University of Montpellier, CNRS, ENSCM, Montpellier, France
[2] ICGM, University of Montpellier, CNRS, ENSCM, Montpellier, France
[*] Corresponding authors: herve.cottet@umontpellier.fr ; laurent.leclercq@umontpellier.fr

Abstract:

Protein adsorption on the inner wall of the fused silica capillary wall is an important concern for capillary electrophoresis (CE) analysis since it is mainly responsible for separation efficiency reduction. Successive Multiple Ionic-polymer Layers (SMIL) are used as capillary coatings to limit protein adsorption, but even low residual adsorption strongly impacts the separation efficiency, especially at high separation voltages. In this work, the influence of the chemical nature and the PEGylation of the polyelectrolyte deposited in the last layer of the SMIL coating was investigated on the separation performances of a mixture of four model intact proteins (myoglobin (Myo), trypsin inhibitor (TI), ribonuclease a (RNAse A) and lysozyme (Lyz)). Poly(allylamine hydrochloride) (PAH), polyethyleneimine (PEI), ε-poly(L-lysine) (εPLL) and α-poly(L-lysine) (αPLL) were compared before and after chemical modification with polyethyleneglycol (PEG) of different chain lengths. The experimental results obtained by performing electrophoretic separations at different separation voltages allowed determining the residual retention factor of the proteins onto the capillary wall via the determination of the plate height at different solute velocities and demonstrated a strong impact of the polycationic last layer on the electroosmotic mobility, the separation efficiency and the overall resolution. Properties of SMIL coatings were also characterized by quartz microbalance and atomic force microscopy, demonstrating a glassy structure of the films.

Keywords: protein adsorption; capillary zone electrophoresis; successive multiple ionic-polymer layer; PEGylated polycation; polyelectrolyte multilayers

Highlights:

- Impact of the last layer on SMIL capillary coating on analytical performances
- Impact of PEGylated last layer on electroosmotic flow and analytical performances
- Impact of the nature of the last polycation layer on SMIL thickness and hydration
- Comparable results between QCM-D and AFM experiment, in agreements with CE findings

1. Introduction

Theoretical separation efficiency in capillary electrophoresis (CE) is ideally controlled by solute axial diffusion [1]. For a globular protein of typical size about 1 nm (molecular diffusion coefficient D of about 2×10^{-10} m^2s^{-1}, apparent electrophoretic mobility of 20 TU (Tiselius Units: 1 TU = 10^{-9} $m^2V^{-1}s^{-1}$) and typical electric field strength of 500 V cm^{-1} corresponding to "typical" 20 kV per 40 cm total capillary length used in this study), about one million theoretical plates are expected in an ideal CE experiment. In practice, the plate number is generally much lower, with typically about a few tens of thousands plates [2-4]. Different factors can explain this reduction, among which radial gradient temperature inside the capillary [5] due to Joule effect and capillary cooling, electromigration dispersion [6,7], capillary coiling [8], or protein adsorption onto the capillary wall [3, 9-13]. Monolayer coatings and successive multiple ionic-polymer layer (SMIL) capillary coatings were developed to limit protein adsorption [14-28]. Pioneered in the late 1960 [29], multilayered polyelectrolyte coatings were rediscovered at the beginning of the 90s by Decher et al. [30, 31] and firstly applied to CE in 1998 [32]. SMIL coatings are built inside the capillary by successive adsorption of oppositely charged polyelectrolytes (PE) onto the capillary wall. SMIL coatings greatly improve the separation repeatability / reproducibility compared to bare fused silica capillary [4, 22, 33-35], but even very small residual protein adsorption can still reduce the separation efficiency [36], with a plate height H increasing with the power 2 of the retention factor k. For a fair comparison of the coating performances between different capillary coatings, and for a valuable quantitative estimation of their performances, it was thus crucial to quantify residual protein adsorption by the determination of the protein retention factor k. We recently demonstrated that this determination can be performed by quantifying protein separation efficiency at different separation voltages. Experimentally, the plate height H obtained for each protein at different separation voltages can be plotted as a function of the protein linear velocity u according to the following law [13, 37]:

$$H = \frac{2D}{u(1+k)} + \frac{d_c^2 u}{D}\frac{k^2}{16(1+k)} + \frac{2}{3}\frac{{d_f}^2 u}{D_s}\frac{k}{1+k} + A \qquad (1)$$

where d_c is the internal diameter of the capillary, u is the linear velocity of the analyte, d_f is the film thickness, D_s is the diffusion coefficient in the stationary phase and A is a constant related to extra column contributions. Knowing that $d_c^2 \gg d_f^2$, the third term related to the resistance in mass transfer in stationary phase can be neglected in equation (1) as a first approximation. Curve fitting of the plate height experimental data is an excellent way to determine k value for each protein on a given capillary coating. In equation (1), D was obtained experimentally by Taylor dispersion

analysis. The determination of *k* values allows a ranking of the capillary coating performances, whatever the electroosmotic mobility values, and thus, whatever the range of protein migration times which can greatly vary with the nature/surface charge of the coating.

Reducing protein adsorption, and thus the retention factor, is probably one of the most critical parameter to improve capillary coatings in CE enabling decreasing the dependency of the peak broadening with increasing separation voltage. The aim of this work was to study the impact of the chemical nature of the last polycationic layer deposited on a 4-layers poly(diallyldimethylammonium chloride) (PDADMAC) / poly(sodium styrene sulfonate) (PSS) sub-structure, on the CE separation performances of a mixture of 4 model intact proteins (myoglobin (Myo), Trypsin inhibitor (TI), ribonuclease A (RNAse A) and lysozyme (Lyz)). PDADMAC, polyallylamine (PAH), polyethyleneimine (PEI), ε-poly(L-lysine) (εPLL) and α-poly(L-lysine) (αPLL) were compared as a last layer, either used as it or after chemical grafting modification with PEG chains of two different lengths (1 kDa and 5 kDa) at various molar proportions. The different CE characteristic parameters and performances (electroosmotic mobility, protein retention factor *k*, constant *A*, separation efficiency, RSD of migration times) were systematically determined to compare all the tested capillaries.

2. Experimental section

2.1. Chemicals and Materials

Reagents. Copper sulfate (99.99% purity), sodium ascorbate (98% purity), tris(benzyltriazolylmethyl) amine (THPTA, 95% purity), sodium nitrate (99.0% purity), 4-(2-hydroxyethyl)-1-piperazineethane sulfonic acid (HEPES, 99.5% purity) and sodium acetate anhydrous (99% purity) were purchased from Sigma-Aldrich (Saint-Quentin-Fallavier, France). Sodium hydroxide (98 % purity) and sodium chloride (99.5% purity) were purchased from Fluka (Saint-Quentin-Fallavier, France). Triethylamine (99% purity) was obtained from Acros Organics (Geel, Belgium). Acetic acid (99.99% purity) was supplied by VWR Chemicals (Rosny-sous-Bois, France). Sodium azide (99.5% purity) was purchased from Merck (Darmstadt, Germany). Dimethylformamide (99.9% purity) was purchased from Carlo Erba Reagents (Val-de-Rueil, France). Trypsin Inhibitor (TI, from soybean, isoelectric point (p*I*): 4.5, purity not indicated by the supplier), Myoglobin (Myo, from equine skeletal muscle, p*I*: 7.3, 95% purity), Ribonuclease A (RNAse A from bovine pancreas, p*I*: 9.3, 60% purity) and Lysozyme (Lyz, from chicken egg white, p*I*: 11.1, 90% purity) were obtained from Sigma-Aldrich (Saint-Quentin-Fallavier, France).

Polymers. Methoxy-(polyethylene glycol)-succinimidyl carboxyl methyl ester (mPEG-NHS-SCM) of 1 kDa (ref.: PLS-215) and 5 kDa (PLS-213) average molar masses; and methoxy-(polyethylene glycol)-alkyne (mPEG-Alkyne) of 1 kDa (PLS-2036) and 5 kDa (PLS-2034) molar masses, were purchased from Creative PEGWorks (Durham, NC, USA). ε-poly(L-Lysine hydrochloride) (εPLL, M_w = 3.5-4.5 kDa) was purchased from Biosynth Carbosynth (Staad, Switzerland). Poly(allylamine hydrochloride) (PAH, M_w = 120-200 kDa) was supplied by Alfa Aesar (Kandel, Germany). Branched poly(ethyleneimine) (PEI, M_w = 750 kDa) and poly(diallyldimethylammonium chloride) (PDADMAC, M_w = 450 kDa) were purchased from Sigma Aldrich (Saint-Quentin-Fallavier, France). α-poly(L-Lysine hydrobromide)-graft-(azidoalkylamide) 10% (αPLL-10%, M_w = 57 kDa) and 20% (αPLL-20%, M_w = 62 kDa) were purchased from Alamanda Polymers (Huntsville, AL, USA). Poly(sodium styrenesulfonate) (PSS, M_w = 70 kDa) was purchased from Acros Organics (Geel, Belgium). Except for PAH and PEI, all reagents and polymers were used as received without any further purification. All aqueous solutions were prepared using deionized water (18 MΩcm^{-1}) delivered by a Synergy UV water purification system (Millipore, Fontenay-sous-Bois, France).

0.1 μm cut-off Durapore membrane filters were purchased from Millipore (Molsheim, France). Dialysis tubings (cut-off: 1, 3.5, 8 and 12–14 kDa) were purchased from Spectrum Labs (San Francisco, CA, USA).

2.2. Proton NMR

^{1}H NMR spectra were recorded on a Varian Unity Inova 400 MHz spectrometer in a D_2O solution, using the resonance of water (4.8 ppm) as chemical shift internal reference. Samples of freeze-dried polymers were dissolved at ca. 1 gL^{-1} in 99.9% D_2O. The dissolution of PEGylated polymers (with 5 kDa PEG chains) in D_2O was performed at 0°C. All the ^{1}H NMR spectra are provided in Supporting Information, Section 1.C (Figure SI 8 to Figure SI 12). ^{1}H NMR integrations were used to estimate the PEGylation ratio achieved at the end of the synthesis (see Table SI1) according to the calculation method described in Figure SI 8.

2.3. Preparative Size Exclusion Chromatography (SEC)

Automated preparative SEC experiments were performed on a General Electric Healthcare Äkta Purifier 100 (Chicago, IL, USA) including a P-900 pump unit and a UV-900 multi wavelength UV-visible detector unit. Separations were carried out on an OHpak SBG Shodex column guard (50 × 6 mm) followed by a 300 × 8 mm SB-805M-HQ Shodex column. The eluent was an aqueous solution of acetic acid (50 mM), sodium acetate (50 mM), sodium chloride (500 mM) and sodium

azide (300 mgL^{-1}), pH 4.8. Prior to use, the eluent was filtered through a 0.1 µm cut-off Durapore membrane. Polymers samples dissolved at 4 gL^{-1} in the eluent were injected by 500-µL successive batches and eluted at 1.0 $mLmin^{-1}$ flow rate. The collected polymer fractions were dialyzed against deionized water, concentrated on a rotatory evaporator, and finally freeze-dried. The resulting powder was stored under inert atmosphere at -20°C.

Prior to use for PEG grafting, commercial PAH and PEI (of polydispersity indexes PDI = 3.5 and 6.0, respectively) were fractionated by preparative SEC, affording samples with final PDI = 1.5 and 1.9, respectively (see Table SI 1, Figure SI 1 to SI 7 for more information).

2.4. Size Exclusion Chromatography coupled to Multi-Angle Laser Light Scattering (SEC-MALLS)

SEC-MALLS analyses were carried out on a Thermo Scientific Dionex Ultimate 3000 instrument (Thermo Fisher Scientific, Waltham, MA, USA) including an auto-sampler & column compartment unit, connected to a Wyatt MiniDawn Treos three-angle laser light scattering detector (41.5°, 90°, and 138.5°) operating at 658 nm (Wyatt Technology Corp., Santa Barbara, CA, USA) and to a Shimadzu RID-20A refractometer (Shimadzu Corp., Kyoto, Japan). Separations were carried out on a 50 × 6 mm OHpak SBG Shodex column guard followed by a 300 × 8 mm SB-805M-HQ Shodex column. The eluent was composed of a mixture of 50 mM acetic acid, 300 mM sodium nitrate and 300 mgL^{-1} sodium azide, pH 3.6. Prior to use, the eluent was filtered through a 0.1 µm cut-off Durapore membrane. 100 µL polymer samples (dissolved at 1 gL^{-1} in the eluent) were injected and eluted at a 1.0 $mLmin^{-1}$ flow rate. Raw instrument data were processed using the Astra software (v6.1.1.17, Wyatt Technology Corp.), analyzing the 5–17 mL elution volume range in all cases.

SEC-MALLS analytic results were used to assess PEG/polycation ratios and to quantify the amount of residual ungrafted mPEG in the grafted polymers (see Sections I.D and I.E in Supporting Information).

2.5. Incremental refractive index $(dn/dc)_\mu$ determination

Incremental refractive indexes $(dn/dc)_\mu$ of polymers were measured at constant chemical potential (μ) on the RID-20A refractometer unit. Mother polymer solutions at 2.0 gL^{-1} in SEC eluent were prepared by weighing the dry polymer and the SEC eluent. Various dilutions of mother polymer solutions in SEC eluent (final polymer concentrations: 0.25, 0.5, 0.75, 1.0, 1.5, and 2.0 gL^{-1}) were then submitted to RID measurement. All molar masses and concentrations used for *dn*/*dc* measurements included the polymer counter-ions (see Figure SI3 to SI7). The values of $(dn/dc)_\mu$

were 0.1887 for εPLL, 0.1731 for αPLL 10%, 0.1837 for αPLL 20%, 0.2125 for PAH and 0.3004 for PEI.

2.6. PEGylation of PAH by NHS activation

HEPES-NaOH buffer pH 7.52 was prepared by mixing HEPES at 30 mM (1.786 g in 250 mL deionized water) with sodium hydroxide at 15 mM (0.1501 g in 250 mL deionized water). In all weighing and transfer operations, the intermediate vessel was rinsed with 5 mL buffer to maximize substrate/reagent recovery into the reaction vessel. In a typical experiment, 32.5 mg (348.6 µmol monomer units) of PAH were dissolved in 5 mL HEPES-NaOH buffer, then the resulting solution was transferred into a 50 mL flask under vigorous stirring for 5 min (the vial used for weighing was subsequently rinsed with 5 mL buffer). 40.1 mg (41.8 µmol endgroups) of mPEG-SCM were added portionwise into the PAH solution. The intermediate vial was rinsed with 5 mL of buffer to transfer the leftover reagent. The flask was closed, and the solution was stirred overnight. The reaction medium was then dialyzed over 48 h against water (1 kDa cutoff tubing) to remove ungrafted mPEG, meanwhile the outer water was renewed 7 times. The solution was then concentrated on a rotatory evaporator and finally freeze-dried overnight. The resulting solid was then characterized by 400 MHz ^{1}H NMR (see Figure SI 8 to SI 12) and by SEC-MALLS (see Figure SI 13 to SI 20). Quantitative data for all examples are gathered in Table SI1.

2.7. Capillary coating procedure

Bare fused silica capillary (purchased from Polymicro Technologies (Phoenix, AZ, USA)) was first activated according to the following procedure: successive flushes (at 96.5 kPa (14.5 psi)) of NaOH (1 M, 10 min, 1 mL in a 1.5 mL glass vial), pure water (5 min, 1 mL in a 1.5 mL glass vial) and construction buffer (HEPES 20 mM, NaOH 10 mM, pH 7.4, 10 min, 1 mL in a 1.5 mL glass vial). A 4-layer SMIL capillary coating, used as a substructure, was obtained by flushing (at 96.5 kPa) with polycation solution (PDADMAC, 3 gL^{-1} in HEPES buffer, 7 min, 200 µL in polypropylene vial), HEPES buffer (3 min, 1 mL in a 1.5 mL glass vial) to remove the excess of polycation, polyanion solution (PSS, 3 gL^{-1} in HEPES buffer, 7 min, 200 µL in polypropylene vial), HEPES buffer (3 min, 1 mL in a 1.5 mL glass vial) to remove the excess of polyanion. To avoid polyelectrolyte contamination, HEPES solutions for PDADMAC and PSS rinsing flushes were stored in different vials. This procedure was repeated once more to obtain the 4-layer SMIL substructure. The fifth layer was deposited by flushing (at 96.5 kPa, 7 min, 200 µL in polypropylene vial) with either PDADMAC, PAH, PEI, εPLL, αPLL (either native or PEGylated), followed by a rinsing step with HEPES buffer (3 min, 1 mL in another 1.5 mL glass vial) and 5

min wait. Finally, the coated capillary was flushed (at 96.5 kPa) with pure water (3 min) and background electrolyte (BGE) (2 M acetic acid, pH 2.2, 10 min) followed by another 5 min wait before analysis.

2.8. Separation of intact proteins by capillary zone electrophoresis

Capillary zone electrophoresis experiments were performed on a P/ACE MDQ Beckman Coulter (Sciex, Villebon-sur-Yvette, France) piloted by 32 Karat software. Analyses were performed on a 40 cm total length capillary (30 cm effective length), with inner (i.d.) and outer (o.d.) diameters of 50 µm (± 0.3 µm) and 363 µm (± 15 µm), respectively. Electrophoretic separations were performed in a 2 M acetic acid BGE, pH 2.2 (6.4 mM ionic strength). BGE was flushed (at 96.5 kPa) for 3 min between each run. Separations were performed at different voltages between ±10 and ±20 kV, with a polarity depending on the capillary surface charge (as indicated on the Figure caption). DMF (0.001% m/v in the BGE) was hydrodynamically injected as EOF marker at 2.7 kPa (0.4 psi) for 2 s, followed by a protein mixture (0.25 gL^{-1} each in the BGE) at 2.7 kPa for 4 s. RNAse A, Lyz, Myo and TI were kept separately in pure water (at 2 gL^{-1}) in the freezer before dilution in the BGE for the preparation of the sample mixture. The temperature of the cartridge was set at 25°C. Detection wavelength was 214 nm.

2.9. Single channel Quartz Crystal Microbalance with Dissipation (QCM-D)

QCM-D experiments were performed on a X1 Single Channel device (from AWSensors, Valencia, Spain), using an "in-flow" QCM cell at 23°C, equipped with a 14 mm diameter quartz sensor coated by SiO_2 and with a fundamental resonance frequency of 5 MHz. The coating procedure was performed on bare sensors first activated by O_2 plasma (5 min, $P(O_2)$ = 0.5 mbar, 80W). Normalized frequency shifts ($\Delta f_n/n$ in Hz) and corresponding normalized dissipation shifts ($\Delta D_n/n$) for the 3rd, 5th, 7th and 9th resonance harmonics (n) were first measured in air, then monitored throughout the experiment. Before starting the SMIL buildup, pure water was flushed at 0.05 $mLmin^{-1}$ until stabilization of QCM signals, followed by flushing with the construction buffer (HEPES 20 mM, NaOH 10 mM, pH 7.4) for 20 to 30 min. The film was assembled by sequential injection of PDADMAC and PSS solutions (at 3 gL^{-1} in construction buffer) for 30 min at 0.05 $mLmin^{-1}$, starting with PDADMAC as first layer. Rinsing with the construction buffer was performed for 30 min between each polyelectrolyte adsorption step. Once a 4-layer SMIL $(PDADMAC/PSS)_2$ was obtained, a differentiated capping layer based either on εPLL or PAH (at 3 gL^{-1} in construction buffer) with PEG grafting ratios of 0, 11 and 20 % was deposited for 30 min at 0.05 $mLmin^{-1}$. After rinsing with the construction buffer, the SMIL-coated QCM sensor

was stabilized in pure water with a 0.05 $mLmin^{-1}$ flow rate. Both the normalized resonance frequency shift ($\Delta f_n/n$ in Hz; related to the mass deposited on the sensor), and the normalized dissipation shift ($\Delta D_n/n$; related to the energy dissipated by the resonator in its direct surrounding), were discussed. High $\Delta D_n/n$ values and $\Delta f_n/n$ spreading are characteristics of a viscoelastic coating, such as hydrated SMIL film structures. Overtones frequency shifts overlap and low dissipation shift values (i.e., when the final $\Delta D_n/n$ divided by the final $\Delta f_n/n$ is equal or lower to 4×10^{-7}) [38] are typical of rigid glassy film structures. In the case of thin rigid films, the mass deposited on the crystal can be calculated from the Sauerbrey equation [39]:

$$\Delta m = -C \times \Delta f_n/n \quad (2)$$

where Δm (in $ngcm^{-2}$) corresponds to the variation of areal mass, C (in $ngcm^{-2}Hz^{-1}$) is the mass-sensitivity constant that depends on crystal property, n is the overtone number and Δf is the frequency shift (in Hz). A typical mass sensitivity constant C = -17.7 $ngcm^{-2}Hz^{-1}$ value can be used for a 5 MHz quartz crystal resonator at room temperature.

The film buildup kinetics was evaluated by plotting the values of $\Delta f_3/3$ and $\Delta D_3/3$ for each layer after HEPES rinsing, as well as the corresponding calculated areal masses deposited on the crystal according to Saurebrey's model. Determination of the film thickness was performed using the QTM software, taking account of all frequency overtones and approximating the SMIL mass density as ρ = 1 gcm^{-3} [40].

2.10. Atomic Force Microscopy (AFM)

Activation and coating of QCM-D sensor were realized as described in Section 2.9. QCM-D sensors were prepared overnight before AFM analysis and kept in water to avoid SMIL retraction. Atomic force microscope measurements were performed using a Multimode 8 Instrument controlled by Nanoscope 5 electronic software. Peak Force Tapping mode cantilevers (Nanosensors) with scanasyst fluid spring (constant near 0.7 N/m) were used for the imaging at approximately 60 kHz in air and water. Images were analyzed using Gwydion software.

3. Results and discussion

In this work, a series of cationic polyelectrolytes, namely PAH, PEI, εPLL or αPLL, were grafted with PEG (1kDa or 5 kDa) at different molar proportions. These polycations were selected because they contain primary amine groups that can be derivatized with lateral PEG chains. PAH, PEI, εPLL were derivatized using the NHS / primary amine reactivity, while αPLL were

derivatized using a click-chemistry approach. The PEG grafted polycations are named "Polycation-g-($mPEG_y$)$_x$" where *y* corresponds to the mPEG length (1kDa or 5 kDa) and *x* is the calculated PEG/polycation molar ratio. Various PEGylation molar ratios were achieved up to 20%. All details about the synthesis, chemical structure and characterization, are given in the experimental sections 2.2 to 2.6 and in the SI (see Table SI 1 and subsequent sections in Supporting Information).

Non-PEGylated and PEGylated PAH, PEI, εPLL or αPLL were used as a last layer deposited on a 4-layer PDADMAC/PSS SMIL sub-structure for capillary coatings, as depicted in Figure 1. The PDADMAC / PSS system was retained as a suitable sub-structure since it was described as a prime SMIL coating for CE applications [35]. To study the impact of the last polycationic layer on separation performances in CE, a mixture of 4 model intact proteins (Myo, RNAse A, Lyz, TI at 0.25 gL^{-1} each in 2 M acetic acid, pH 2.2) was selected.

3.1. Influence of the polycation nature on the last layer on the H=f(u) curve and resolution

Before studying the impact of the PEGylation of the polycationic last layer on the CE separation performances, the 5-layer SMIL coating terminating with the non-PEGylated PDADMAC, PAH, PEI, εPLL or αPLL were first compared. The electropherograms (five repetitions) obtained for the separation of the protein mixture at different separation voltages (i.e., -20 kV, -17.5kV, -15kV, -12.5kV and -10 kV, with typical electric currents of 18.1 µA, 15.7 µA, 13.4 µA, 11.0 µA and 8.8 µA, respectively) are shown in Supporting Information (see Figure SI 21 to Figure SI 25). An example of electropherograms, repetitions obtained at -10 kV is displayed in Figure 2A. Excellent repeatabilities were generally obtained as demonstrated by the very low RSDt_m (typically lower than 0.6%) on migration times at -10 kV and -20 kV (see Table 1 for numerical data). The repeatability followed this ranking: PEI > PDADMAC ~ PAH > αPLL ~ εPLL. Lower stability was observed for PLL, and especially for εPLL at -10 kV. To get more information about the performances of the capillary coatings, the *H=f(u)* plots were systematically investigated by measuring the separation efficiency (plate height) at different separations voltages. Figure 2B shows typical *H=f(u)* plots in the case of Myo for all the polycations tested as a last layer (see Figure SI 26 for the experimental plots on TI, RNAse A and Lyz). Using equation (1), all the *H=f(u)* plots were fitted taking *k* and *A* as variable parameters and by neglecting the third term in the right-hand side of the equation which is related to the resistance in mass transfer in stationary phase. Table 1 gathers the numerical adjusted data for *k* and *A* for the 4 proteins. From Figure 2A, it clearly appears that PAH, and to a lower extend PDAMAC are the best coatings leading to the

lower *H* values (see Figure SI 26). This conclusion is also confirmed by the ranking based on the *k* values (see Table 1): PDADMAC (6.5×10^{-2}) ~ PAH (6.9×10^{-2}) < PEI (7.3×10^{-2}) < αPLL (7.5×10^{-2}). Regarding εPLL, poor curve fitting was obtained together with much lower repeatabilities on separation efficiency (see larger error bars in Figure 2B) which can be considered as a signature of a lower stability of the coating. This finding can be explained by the low polymer molar mass (ca. 4000 g mol^{-1}) of εPLL compared to that of the other polymers (10 to 100 times longer chains) that generated less robust SMIL coatings. The low *k* value obtained for εPLL (3.8×10^{-2}) should be balanced by the much higher *A* value (6.9 µm). The *A* value is supposed to incorporate all constant extra-column effects but the contribution to the *A* value in regard to the coating properties remains unclear.

SMIL coatings induced differences in the electroosmotic mobility and thus migration time. Therefore, the impact of the last polycationic layer was investigated on peak resolution (R_s) based on the Myo / RNAse A pair (see Figure 2C). R_s depends both on the migration times and the separation efficiency, as shown in equation 3:

$$R_s = \frac{1}{4} \times \frac{\Delta\mu_{ep}}{< \mu_{app} >} \times \sqrt{N} \qquad (3)$$

where $<\mu_{app}>$ is the average apparent electrophoretic mobility of the two analytes (in TU), $\Delta\mu_{ep}$ is the difference in effective electrophoretic mobility between the two analytes and *N* is the average plate number. The highest R_s values were obtained with the PAH polycation followed by PDADMAC or εPLL (see Figure 2C). Despite the lowest separation efficiencies obtained with εPLL, the resolution loss due to higher peak broadening was balanced by the decrease of the electroosmotic flow (μ_{eo}(εPLL) = -40.7 TU *vs* μ_{eo}(PDADMAC) = -45.5 TU) which increased the apparent selectivity and migration times. A diminution of the resolution was observed for all the coatings when the applied voltage increased (increasing *u*) since the experimental data are located in the ascending part of the *H*=f(*u*) curve. As a conclusion of this first part, it seems that PAH is the best polycation for the last layer, and therefore the best candidate for subsequent PEGylation.

3.2. Investigating SMIL growth by QCM-D

The SMIL film growth was investigated by QCM-D. Figure 3 shows the dissipation and frequency shifts of the 3rd harmonic during the SMIL construction. Since films terminated by PEI and αPLL

presented similar behavior as PAH, but with lower analytical efficiency, only films terminated by PAH were investigated by QCM-D. Frequency shifts were measured at each injection step of oppositely charged polyelectrolyte (see Section 3 in Supporting Information), signaling the adsorption of the next polyelectrolyte layer by charge overcompensation promoting [30]. The first increment corresponds to PDADMAC (at 3 gL^{-1} in 20 mM HEPES) adsorption onto the bare sensor, followed by rinsing with 20 mM HEPES. Frequency and dissipation shift values of the first step were larger than those of following steps since the adsorption onto the bare QCM sensor is different than onto polyelectrolytes. Average PDADMAC and PSS shift in frequency were 9 Hz and 2 Hz per step, respectively, showing growth of very thin film. As observed in Figure SI 32, low final frequency (-27 Hz) and dissipation shift (3.4×10^{-7}) for the $(PDADMAC/PSS)_2$ SMIL indicated thin films, while overlapping overtones indicated rigid properties. Due to their high linear charge density, PDADMAC and PSS multilayered films are known to form thin and rigid films in low ionic strength conditions (typically 15 mM NaCl [41]). As the Sauerbrey equation is applicable for thin rigid films (see Section 2.9, eq. 2), an approximated deposited areal mass was calculated for the $(PDADMAC/PSS)_2$ SMIL coating: a frequency shift of ≈ -26.98 Hz was found, leading to 478 $ngcm^{-2}$ deposited areal mass (corresponding to a film thickness of 4.5 nm), as presented in Table 2.

Next, the influence of the last deposited cationic layer on the film growth was investigated. εPLL deposition showed the smallest final frequency shift and final dissipation, corresponding to 98 $ngcm^{-2}$ deposited areal mass. In the case of PDADMAC, the deposited areal mass was higher (121 $ngcm^{-2}$). In contrast, the deposition of PAH as a last layer led to harmonic differentiation and a concomitant increase in dissipation values (Figure SI 33), indicating a change in the viscoelastic properties of the film, attributed to a more hydrated structure. Yet, the ratio of final $\Delta f_3/3$ divided by final $\Delta D_3/3$ was around 1.5×10^{-7}, indicating that the Sauerbrey equation was still valid for this film, with a calculated deposited areal mass of 301 $ngcm^{-2}$. For all systems, and with the film volumic mass (ρ) approximated to 1 gcm^{-3}, the thickness was determined using QTM software as about 7 nm (see exact values in Table 2).

AFM analyses were performed on bare and $(PDADMAC/PSS)_{2.5}$ SMIL coated QCM-D sensor in air and water medium to characterize SMIL covering. As shown in Figure SI 37, no significant impact was observed in the case of bare sensor when analysis was performed either in air (roughness of 0.9 nm) or in water (roughness of 1.1 nm). Comparing with the SMIL coated sensor in water (Figure SI 38), an increase of 2.3 nm in rugosity was observed, related to the presence of the SMIL at the surface. Finally, AFM experiment was performed on the same QCM-D sensor,

after complete evaporation of water (Figure SI 39). Bare silica (dark area) was observed on the left of the picture, while the dried SMIL coating remained on the right. The in-between light zone corresponds to SMIL retractation. To measure SMIL height, topographic measurement was performed on the bare silica zone and on the SMIL coating zone, leading to average 8.7 ± 3.8 nm and 7.2 ± 5.0 nm differences (see Table SI2), in agreement with the value obtained by QCM-D experiment (6.8 nm).

To conclude, with average film thickness of around 7 nm and final dissipation below 7×10^{-6}, all films showed rigid properties. PDADMAC and εPLL yielded thinner film coating, with lower deposited areal mass and dissipation shift than PAH. The glassy nature of these films contributes to refraining any diffusion of proteins within the multilayer, while the SMIL's polycationic last layer grants antifouling properties, as experimented in CE (Figure 2). However, the low molar mass of εPLL led to less robust films and thus to lower repeatability in CE measurements [36, 42]. When PAH was used as the last layer, higher dissipation shift and higher deposited masses were observed, but similar or slightly higher CE performances were obtained compared to PDADMAC.

Due to thin film growth, rigid behavior, excellent analytical properties and ease of functionalization, PAH was selected as the capping layer reference. In the following, PEGylation of PAH, which is known to improve antifouling properties [43-52], was investigated, and the impact of PEGylation on electroosmotic mobility and CE separations was discussed.

3.3. Influence of the PEGylation density and length on electroosmotic flow mobility (μ_{eo})

PAH was grafted with PEG chains of two different lengths (1 kDa and 5 kDa) at various ratios (see Section 2.6 for polymer synthesis). PEGylated PAH were prepared from 1 kDa PEG chains (targeting 10% and 20% grafting ratios) and from 5 kDa PEG chains (targeting 1%, 2%, 3.5%, 5%, 7.5%, 10%, 20% and 30% grafting ratios). Effective % of PEGylation was measured by ^{1}H NMR or SEC/MALLS, as described in Sections 2.2 and 2.4, and results were gathered in Table SI 1.

As shown in Figure 4, no influence of the PEGylation of the PAH last layer on the EOF was observed for 1 kDa PEG lateral chains: μ_{eo} was found stable at ≈ -47 TU, even at 23.5% grafting proportion. In contrast, in the case of PAH grafted with 5 kDa mPEG, PEGylation strongly impacted the EOF, even at the lowest PEG ratio. This is in good agreement with the hydrodynamic diameter of a 5kDa PEG (≈ 6 nm [53]) which is higher than the Debye length (4 nm at I = 6.4 mM

ionic strength, 2 M acetic acid BGE), while the typical size of 1kDa PEG chain (around 1 nm [53]) is significantly smaller than the Debye length. The impact of PEGylation on the EOF is based on the hydrodynamic screening of the charges contained in the double layer by the PEG chains. This hydrodynamic screening is only effective when the PEG dimension is larger than the Debye length in the experimental conditions.

Since the electrophoretic mobility (μ_{ep}) of the four proteins tested were 23.7 TU for TI, 27.2 TU for Myo, 28.2 TU for RNAse and 31.6 TU for Lyz, the electrical polarity must be reversed from 5kDa mPEG PAH with grafting ratio equal or higher than 5%. This leads to a complete inversion of the protein migration order. A plateau was reached when PEGylation density was higher than 11%, where essentially a neutral coating behavior was observed ($\mu_{eo} \approx$ -2 TU). PEGylation was also performed on PEI and similar impact on EOF was observed (see Figure 4), but with a faster EOF decrease with the grafting density of the 5 kDa mPEG.

3.4. Impact of the PEGylation of PAH on k and R_s

Figure 5A shows the impact of PEGylation for the PAH grafted with 1kDa PEG chains in the last layer. A slight reduction of μ_{eo} was observed (≈ -41.5 TU). However, intra-capillary repeatability was lower (see RSD_{tm} values in Table 3). In contrast, little impurity peaks around the Lyz peak were detected in the case of PAH-g-$(mPEG_{1kDa})_{0.235}$ in the last layer unlike PAH, due to better selectivity due to the slight EOF reduction.

Figure 5B shows the impact of PEGylation for the PAH grafted with 5kDa PEG chains in the last layer. Interestingly, SMIL with PAH-g-$(mPEG_{5kDa})_{0.021}$ gave similar μ_{eo} than PAH-g-$(mPEG_{1kDa})_{0.138 \text{ and } 0.235}$, but with better repeatability. SMIL with PAH-g-$(mPEG_{5kDa})_{0.11}$ showed a quasi-neutral behavior coated capillary with μ_{eo} at ≈ -5.5 TU. The order of detection of the proteins was thus reversed using positive polarity, and the analysis time was drastically reduced (from 12 min for the non-PEGylated PAH to only 7 min for the PAH-g-$(mPEG_{5kDa})_{0.11}$) in the last layer.

Regarding the impact of PEGylation on *H*, 1kDa PEGylated PAH led to lower average *k* values but slightly higher *A* values compared to the unmodified PAH, as shown for instance in Figure 6A for Myo, Figure 6B for Lyz and Table 3. Average *k* value (tested on the four proteins) was 7 × 10^{-2}, 4.4 × 10^{-2} and 6.05 × 10^{-2} for PAH, (PAH-g-$(mPEG_{1kDa})_{0.138})_1$ and (PAH-g-$(mPEG_{1kDa})_{0.235})_1$, respectively. Average *A* values changed from 1.9 µm for PAH to 4.4 µm for 13.8% mPEG grafted PAH and 3.3 µm for 23.5% mPEG grafted PAH. On the whole, the separation efficiencies were very similar to those obtained with unmodified PAH, but the

resolution was significantly higher with 1kDa PEGylation (see Figure 6C), especially at high voltage due to flatter H=f(u) curve and slightly lower EOF.

Increasing mPEG length from 1kDa to 5kDa was first detrimental on the average k value at intermediate grafting ratio ($k = 9.4 \times 10^{-2}$ for 2.1% PEG) but reached similar value ($k = 4.8 \times 10^{-2}$) for higher ratios (11% PEG). Higher average A values were obtained, i.e. 4.65 µm at 2.1% and 5.3 µm at 11%. This non-linear effect of PEGylation on both the slope (k) and the constant value A of the H=f(u) curve may be not only related to residual protein adsorption. The coating homogeneity may also affect the characteristics of H=f(u) curve.

On the whole, the PEGylation of the PAH last layer was found to lead to much flatter H=f(u) curve, except at intermediate 5 kDa grafting ratio (2.1%). Therefore, the resolution was much less affected by increasing voltages on PEGylated SMIL compared to the non-PEGylated PAH last layer (see the variation of the resolution between Myo and RNAse A with the voltage on Figure 6 C).

Figure 7 compares the $(PDADMAC/PSS)_2$-$(PAH)_1$ SMIL building to two other films obtained with PEGylated PAH as the last layer. The PAH backbone interacts electrostatically with the last PSS layer, while neutral mPEG pendant chains in PEGylated PAH could extend at the SMIL/BGE interface. As the last layer, PAH (unmodified or PEGylated) led to films with slightly less rigid behavior and frequency overtone spreading (Figures 3 and SI 33) compared to PDADMAC last layered SMIL. When adsorbing PEGylated PAH chains on SMIL, two adverse effects can be inferred: on the one hand the molar mass of each polycationic chain is significantly increased by grafted neutral pendant chains, leading to thicker films and larger mass deposition. On the other hand, the charge density of grafted PAH is decreased while steric hindrance increases, which can limit polymer chain adsorption and lead to thinner films. When comparing SMILs capped by either unmodified PAH or 5kDa PEGylated PAH (11% grafting ratio) as the last layer, the latter exhibited a larger frequency shift concomitant with a larger overtone spread (Figure SI35); however similar dissipation values were observed in both cases. In contrast, the frequency shift, overtone spreading (Figure SI 36) and dissipation values, were similar or inferior to that of PAH when 1 kDa PEGylated PAH (20% grafting rate) were adsorbed as a capping layer. These results indicate that thicker films are promoted by PAH bearing longer pendant chains with a moderate grafting degree while thinner films are formed with shorter pendant chains and higher grafting degree. Since the final dissipation and frequency shifts obtained for all films remained in the rigid domain, the Sauerbrey equation was applied to estimate deposited areal masses and the corresponding thicknesses were calculated (Table 4). While films capped with PAH and 1 kDa

PEGylated PAH chains (23% grafting rate) reached similar thicknesses (≈ 7 nm), demonstrating that less chain adsorption had occurred with the latter, the SMIL capped with 5 kDa PEGylated PAH (11% grafting rate) exhibited a deposited areal mass 50 % higher, leading to a ≈ 11 nm thick film. In that case, the thickness of the last deposited layer accounts thus for around 7 nm, a result that confirms that the mPEG impact on EOF was observed for PEG chains longer than the Debye length (Figure 4). Such a significant increase in the film thickness when 5 kDa PEGylated PAH (11% grafting rate) was deposited, suggests that mPEG chains adopt a non-collapsed conformation on top of the coating. Combination of the rigid film structure of $(PDADMAC/PSS)_2$, known for its high stability, robustness and analytical separation efficiency [3, 4, 36], with a slightly hydrated polycation in the last layer where the water thin layer reduced adhesion or adsorption phenomena [54-56], is thus key to coatings with antifouling properties.

4. Conclusion

The first step of this work was to investigate the impact of the last polycationic layer on separation performances in CE using SMIL coated capillaries. For that purpose, five different polyelectrolytes were tested on a $(PDADMAC/PSS)_2$ SMIL coating, namely PDADMAC, PAH, PEI, εPLL and αPLL. With similar properties as PDADMAC, PAH was found the best candidate to investigate the impact of PEGylation in the last layer. 5 kDa PEGylation generated reduced EOF, even at low PEG ratios (typically between 1 and 5 % grafting), while the impact of 1 kDa PEGylation on EOF was much lower even at high grating rates (i.e. 10-25%), with a decrease of the electroosmotic mobility by only about 5%. This finding can be explained by the hydrodynamic screening of the PEG chains in the electrical double layer by sufficiently long PEG chains. An electroosmotic mobility plateau was reached for 5 kDa PEG chains, when the PEGylation rate was above 11%. The SMIL coating then adopts a neutral behavior with very low electroosmotic mobility (~ 2 TU) and a reverse migration order of detection of the proteins.

Regarding the analytical behavior of PEGylated last layered SMIL, flatter H=f(u) curves were generally obtained leading to lower k values in agreement with antifouling properties. However, a slight increase of the A values was observed, for unknown reason. On the whole, a lower impact of increasing applied separation voltage (electric field strength) on the separation performances could be obtained using the PEGylated SMIL. The use of $(PDADMAC/PSS)_2$-$(PAH\text{-}g\text{-}(mPEG_{5kDa})_{0.11})_1$ SMIL coating is a very convenient way to build a performant and almost neutral coating, which is not possible to obtain with classical SMIL coatings terminating with positive or negative surface charges. In conclusion, SMILs with PEGylated polycations as the last layer can

be used to improve the CE resolution via EOF modulation without compromising the separation efficiency; or as an alternative to neutral coatings for 5kDa PEGylated last layer. As a perspective, it would be interesting to study and to better understand the contribution coming from capillary coatings in the constant term of the H=f(u) curve.

Acknowledgement

This work was supported by the CNRS, the french Ministry of Research (MESR) and the ANR (grant ANR-20-CE92 SMIL E, for L.D.). The authors thank the Technological Center in Micro and nanoelectronics (CTM) in Montpellier for AFM experiments.

References

[1] J.W. Jorgenson, K. DeArman. Lukacs, Zone electrophoresis in open-tubular glass capillaries, Anal. Chem. 53 (1981) 1298–1302. https://doi.org/10.1021/ac00231a037

[2] M. Pattky, C. Huhn, Advantages and limitations of a new cationic coating inducing a slow electroosmotic flow for CE-MS peptide analysis: a comparative study with commercial coatings, Anal Bioanal Chem. 405 (2013) 225–237. https://doi.org/10.1007/s00216-012-6459-8

[3] L. Leclercq, M. Morvan, J. Koch, C. Neusüß, H. Cottet, Modulation of the electroosmotic mobility using polyelectrolyte multilayer coatings for protein analysis by capillary electrophoresis, Anal. Chim. Acta. 1057 (2019) 152–161. https://doi.org/10.1016/j.aca.2019.01.008

[4] S. Roca, L. Dhellemmes, L. Leclercq, H. Cottet, Polyelectrolyte multilayers in capillary electrophoresis, ChemPlusChem. 87 (2022). https://doi.org/10.1002/cplu.202200028

[5] X. Xuan, D. Li, Band-broadening in capillary zone electrophoresis with axial temperature gradients, Electrophoresis 26 (2005) 166–175. https://doi.org/10.1002/elps.200406141

[6] J.L. Beckers, UV detection in capillary zone electrophoresis peaks or dips - that is the question, J. Chromatogr. A 679 (1994) 153–165. https://doi.org/10.1016/0021-9673(94)80322-6

[7] Z. Malá, P. Gebauer, P. Boček, New methodology for capillary electrophoresis with ESI-MS detection: Electrophoretic focusing on inverse electromigration dispersion gradient. High-sensitivity analysis of sulfonamides in waters, Anal. Chim. Acta. 935 (2016) 249–257. https://doi.org/10.1016/j.aca.2016.06.016

[8] V. Kašička, Z. Prusík, B. Gaš, M. Štědrý, Contribution of capillary coiling to zone dispersion in capillary zone electrophoresis, Electrophoresis 16 (1995) 2034–2038. https://doi.org/10.1002/elps.11501601332

[9] M.G. Khaledi, High-performance capillary electrophoresis theory, techniques, and applications, John Wiley & Sons, Inc., (1998), vol. 146, p. 303-401

[10] S. Ghosal, Fluid mechanics of electroosmotic flow and its effect on band broadening in capillary electrophoresis, Electrophoresis 25 (2004) 214–228. https://doi.org/10.1002/elps.200305745

[11] S. Ghosal, Electrokinetic flow and dispersion in capillary electrophoresis, Annu. Rev. Fluid Mech. 38 (2006) 309–338. https://doi.org/10.1146/annurev.fluid.38.050304.092053

[12] B. Gaš, M. Štědrý, E. Kenndler, Peak broadening in capillary zone electrophoresis, Electrophoresis 18 (1997) 2123–2133. https://doi.org/10.1002/elps.1150181203

[13] M.R. Schure, A.M. Lenhoff, Consequences of wall adsorption in capillary electrophoresis: theory and simulation, Anal. Chem. 65 (1993) 3024–3037. https://doi.org/10.1021/ac00069a015

[14] L. Hajba, A. Guttman, Continuous-flow-based microfluidic systems for therapeutic monoclonal antibody production and organ-on-a-chip drug testing, J. Flow Chem. 7 (2017) 118–123. https://doi.org/10.1556/1846.2017.00014

[15] V. Dolník, Capillary electrophoresis of proteins 2005–2007, Electrophoresis 29 (2008) 143–156. https://doi.org/10.1002/elps.200700584

[16] P.G. Righetti, C. Gelfi, B. Verzola, L. Castelletti, The state of the art of dynamic coatings, Electrophoresis 22 (2001) 603–611. https://doi.org/10.1002/1522-2683(200102)22:4<603::AID-ELPS603>3.0.CO;2-N

[17] C.A. Lucy, A.M. MacDonald, M.D. Gulcev, Non-covalent capillary coatings for protein separations in capillary electrophoresis, J. Chromatogr. A 1184 (2008) 81–105. https://doi.org/10.1016/j.chroma.2007.10.114

[18] K.S. McMillan, A.G. McCluskey, A. Sorensen, M. Boyd, M. Zagnoni, Emulsion technologies for multicellular tumour spheroid radiation assays, Analyst 141 (2016) 100–110. https://doi.org/10.1039/C5AN01382H

[19] S. Štěpánová, V. Kašička, Recent applications of capillary electromigration methods to separation and analysis of proteins, Anal. Chim. Acta 933 (2016) 23–42. https://doi.org/10.1016/j.aca.2016.06.006

[20] S. Štěpánová, V. Kašička, Applications of capillary electromigration methods for separation and analysis of proteins (2017–mid 2021) – A review, Anal. Chim. Acta. 1209 (2022) 339447. https://doi.org/10.1016/j.aca.2022.339447

[21] C. Renard, L. Leclercq, A. Stocco, H. Cottet, Superhydrophobic capillary coatings: Elaboration, characterization and application to electrophoretic separations, J. Chromatogr. A 1603 (2019) 361–370. https://doi.org/10.1016/j.chroma.2019.06.035

[22] S. Bekri, L. Leclercq, H. Cottet, Polyelectrolyte multilayer coatings for the separation of proteins by capillary electrophoresis: Influence of polyelectrolyte nature and multilayer crosslinking, J. Chromatogr. A 1399 (2015) 80–87. https://doi.org/10.1016/j.chroma.2015.04.033

[23] A. Pallotta, I. Clarot, J. Beurton, B. Creusot, T. Chaigneau, A. Tu, P. Lavalle, A. Boudier, Analytical strategy for studying the formation and stability of multilayered films containing gold nanoparticles, Anal Bioanal Chem. 413 (2021) 1473–1483. https://doi.org/10.1007/s00216-020-03113-6

[24] L. Villemet, A. Cuchet, C. Desvignes, C.E. Sänger–van de Griend, Protein mapping of peanut extract with capillary electrophoresis, Electrophoresis. 43 (2022) 1027–1034. https://doi.org/10.1002/elps.202100004

[25] M. Horká, J. Šalplachta, P. Karásek, M. Roth, Sensitive identification of milk protein allergens using on-line combination of transient isotachophoresis/micellar electrokinetic chromatography and capillary isoelectric focusing in fused silica capillary with roughened part, Food Chem. 377 (2022) 131986. https://doi.org/10.1016/j.foodchem.2021.131986

[26] K. Michalikova, E. Dominguez-Vega, G.W. Somsen, R. Haselberg, Middle-up characterization of the monoclonal antibody infliximab by capillary zone electrophoresis-mass spectrometry, LC GC Eur., 32 (3) (2019), pp. 130-137.

[27] V. Šolínová, P. Tůma, M. Butnariu, V. Kašička, D. Koval, Covalent anionic copolymer coatings with tunable electroosmotic flow for optimization of capillary electrophoretic separations, Electrophoresis. 43 (2022) 1953–1962. https://doi.org/10.1002/elps.202200130

[28] R. Konášová, M. Butnariu, V. Šolínová, V. Kašička, D. Koval, Covalent cationic copolymer coatings allowing tunable electroosmotic flow for optimization of capillary electrophoretic separations, Anal. Chim. Acta. 1178 (2021) 338789. https://doi.org/10.1016/j.aca.2021.338789

[29] R.K. Iler, Multilayers of colloidal particles, J. Colloid Interface Sci. 21 (1966) 569–594. https://doi.org/10.1016/0095-8522(66)90018-3

[30] G. Decher, J.D. Hong, Buildup of ultrathin multilayer films by a self-assembly process: II. Consecutive adsorption of anionic and cationic bipolar amphiphiles and polyelectrolytes on charged surfaces, Ber. Bunsenges. Phys. Chem. 95 (1991) 1430–1434. https://doi.org/10.1002/bbpc.19910951122

[31] G. Decher, Fuzzy Nanoassemblies: Toward layered polymeric multicomposites, Science. 277 (1997) 1232–1237. https://doi.org/10.1126/science.277.5330.1232

[32] H. Katayama, Y. Ishihama, N. Asakawa, Stable cationic capillary coating with successive multiple ionic polymer layers for capillary electrophoresis, Anal. Chem. 70 (1998) 5272–5277. https://doi.org/10.1021/ac980522l

[33] R. Nehmé, C. Perrin, V. Guerlavais, J.-A. Fehrentz, H. Cottet, J. Martinez, H. Fabre, Use of coated capillaries for the electrophoretic separation of stereoisomers of a growth hormone secretagogue, Electrophoresis 30 (2009) 3772–3779. https://doi.org/10.1002/elps.200900093

[34] R. Nehmé, C. Perrin, H. Cottet, M.-D. Blanchin, H. Fabre, Stability of capillaries coated with highly charged polyelectrolyte monolayers and multilayers under various analytical conditions—Application to protein analysis, J. Chromatogr. A 1218 (2011) 3537–3544. https://doi.org/10.1016/j.chroma.2011.03.040

[35] T.W. Graul, J.B. Schlenoff, Capillaries modified by polyelectrolyte multilayers for electrophoretic separations, Anal. Chem. 71 (1999) 4007–4013. https://doi.org/10.1021/ac990277l

[36] L. Leclercq, C. Renard, M. Martin, H. Cottet, Quantification of adsorption and optimization of separation of proteins in capillary electrophoresis, Anal. Chem. 92 (2020) 10743–10750. https://doi.org/10.1021/acs.analchem.0c02012

[37] M. J. E. Golay, Theory of chromatography in open and coated tubular columns with round and rectangular cross-sections, Gas Chromatography 1958, Academic Press, New York, 1958, 36-55

[38] I. Reviakine, D. Johannsmann, R.P. Richter, Hearing what you cannot see and visualizing what you hear: interpreting quartz crystal microbalance data from solvated interfaces, Anal. Chem. 83 (2011) 8838–8848. https://doi.org/10.1021/ac201778h

[39] S. Bruckenstein, M. Shay, Experimental aspects of use of the quartz crystal microbalance in solution, Electrochim. Acta 30 (1985) 1295–1300. https://doi.org/10.1016/0013-4686(85)85005-2

[40] A.E. El Haitami, D. Martel, V. Ball, H.C. Nguyen, E. Gonthier, P. Labbé, J.-C. Voegel, P. Schaaf, B. Senger, F. Boulmedais, Effect of the supporting electrolyte anion on the thickness of PSS/PAH multilayer films and on their permeability to an electroactive probe, Langmuir 25 (2009) 2282–2289. https://doi.org/10.1021/la803534y

[41] M. Elżbieciak-Wodka, M. Kolasińska-Sojka, P. Nowak, P. Warszyński, Comparison of permeability of poly(allylamine hydrochloride)/and poly(diallyldimethylammonium chloride)/poly(4-styrenesulfonate) multilayer films: Linear vs. exponential growth, J. Electroanal. Chem. 738 (2015) 195–202. https://doi.org/10.1016/j.jelechem.2014.11.035

[42] L. Pei, C.A. Lucy, Insight into the stability of poly(diallydimethylammoniumchloride) and polybrene poly cationic coatings in capillary electrophoresis, J. Chromatogr. A 1365 (2014) 226–233. https://doi.org/10.1016/j.chroma.2014.09.013

[43] M. Hedayati, D.F. Marruecos, D. Krapf, J.L. Kaar, M.J. Kipper, Protein adsorption measurements on low fouling and ultralow fouling surfaces: A critical comparison of surface characterization techniques, Acta Biomater. 102 (2020) 169–180. https://doi.org/10.1016/j.actbio.2019.11.019

[44] W.-L. Chen, R. Cordero, H. Tran, C.K. Ober, *50th Anniversary Perspective* : Polymer brushes: novel surfaces for future materials, Macromolecules 50 (2017) 4089–4113. https://doi.org/10.1021/acs.macromol.7b00450

[45] C.-M. Xing, F.-N. Meng, M. Quan, K. Ding, Y. Dang, Y.-K. Gong, Quantitative fabrication, performance optimization and comparison of PEG and zwitterionic polymer antifouling coatings, Acta Biomater 59 (2017) 129–138. https://doi.org/10.1016/j.actbio.2017.06.034

[46] C. Zhang, J. Yuan, J. Lu, Y. Hou, W. Xiong, H. Lu, From neutral to zwitterionic poly(α-amino acid) nonfouling surfaces: Effects of helical conformation and anchoring orientation, Biomaterials 178 (2018) 728–737. https://doi.org/10.1016/j.biomaterials.2018.01.052

[47] B.L. Leigh, E. Cheng, L. Xu, A. Derk, M.R. Hansen, C.A. Guymon, Antifouling photograftable zwitterionic coatings on PDMS substrates, Langmuir 35 (2019) 1100–1110. https://doi.org/10.1021/acs.langmuir.8b00838

[48] X. Lin, P. Jain, K. Wu, D. Hong, H.-C. Hung, M.B. O'Kelly, B. Li, P. Zhang, Z. Yuan, S. Jiang, Ultralow fouling and functionalizable surface chemistry based on zwitterionic carboxybetaine random copolymers, Langmuir 35 (2019) 1544–1551. https://doi.org/10.1021/acs.langmuir.8b02540

[49] R.J. Smith, M.G. Moule, P. Sule, T. Smith, J.D. Cirillo, J.C. Grunlan, Polyelectrolyte multilayer nanocoating dramatically reduces bacterial adhesion to polyester fabric, ACS Biomater. Sci. Eng. 3 (2017) 1845–1852. https://doi.org/10.1021/acsbiomaterials.7b00250

[50] F. Boulmedais, B. Frisch, O. Etienne, P. Lavalle, C. Picart, J. Ogier, J.-C. Voegel, P. Schaaf, C. Egles, Polyelectrolyte multilayer films with pegylated polypeptides as a new type of anti-microbial protection for biomaterials, Biomaterials. 25 (2004) 2003–2011. https://doi.org/10.1016/j.biomaterials.2003.08.039

[51] Z. Zhang, M. Moxey, A. Alswieleh, A.J. Morse, A.L. Lewis, M. Geoghegan, G.J. Leggett, Effect of salt on phosphorylcholine-based zwitterionic polymer brushes, Langmuir. 32 (2016) 5048–5057. https://doi.org/10.1021/acs.langmuir.6b00763

[52] C. Wang, G.K. Such, A. Widjaya, H. Lomas, G. Stevens, F. Caruso, S.E. Kentish, Click poly(ethylene glycol) multilayers on RO membranes: Fouling reduction and membrane characterization, Journal of Membrane Science. 409–410 (2012) 9–15. https://doi.org/10.1016/j.memsci.2012.02.049

[53] S. Liu, D. Guo, G. Xie, Nanoscale lubricating film formation by linear polymer in aqueous solution, J. Appl. Phys. 112 (2012) 104309. https://doi.org/10.1063/1.4765674

[54] J. Peng, Y. Su, Q. Shi, W. Chen, Z. Jiang, Protein fouling resistant membrane prepared by amphiphilic pegylated polyethersulfone, Bioresour. Technol. 102 (2011) 2289–2295. https://doi.org/10.1016/j.biortech.2010.10.045

[55] Y.P. Tang, J.X. Chan, T.S. Chung, M. Weber, C. Staudt, C. Maletzko, Simultaneously covalent and ionic bridging towards antifouling of GO-imbedded nanocomposite hollow fiber membranes, J. Mater. Chem. A. 3 (2015) 10573–10584. https://doi.org/10.1039/C5TA01715G

[56] Y.-J. Shih, Y. Chang, Tunable blood compatibility of polysulfobetaine from controllable molecular-weight dependence of zwitterionic nonfouling nature in aqueous solution, Langmuir (2010) 9. https://doi.org/10.1021/la103186y

Captions to Figures and Tables:

Figure 1. Schematic representation of SMIL coatings used in this work based on $(PDADMAC/PSS)_2$ substructure. The last polycationic layer can be composed of unmodified PDADMAC, PAH, PEI, εPLL and αPLL, or their respective PEGylated chains with different chain lengths.

Figure 2. Impact of the nature of the last layer on protein separation at -10kV (A), on the *H*=f(*u*) curve in the case of Myo (B) and on the resolution of the Myo / RNAse A pair (C). Experimental conditions: $(PDADMAC/PSS)_2$-$(Polycation)_1$ SMIL coated capillary, 40 cm total length (30 cm to detector) × 50 µm i.d. BGE: 2 M acetic acid, pH 2.2. Hydrodynamic injection of proteins at 0.25 gL^{-1} each in BGE: 2.7 kPa, 4s (0.61% V_{tot}). Co-injection of 0.001% DMF in BGE (w/w): 2.7 kPa, 0.4s. Protein mixture: (1) TI, (2) Myo, (3) RNAse A and (4) Lyz. Applied voltages: -10kV, -12.5kV, -15kV, -17.5kV and -20kV. Temperature: 25°C. See Section 2.7 for the coating procedure.

Figure 3. Evolution of frequency (continuous lines) and dissipation (dashed lines) shifts for the 3rd harmonic during SMIL construction procedure in QCMD. Experimental conditions: $(PDADMAC/PSS)_2$-$(Polycation)_1$ SMIL deposited on a silica-coated QCM sensor. Hydrodynamic flow: 0.05 $mLmin^{-1}$. Temperature: 23°C. Average $(PDADMAC/PSS)_2$ layers construction in grey. See Section 2.9 for the coating procedure.

Figure 4. Impact of the PAH and PEI PEGylated polycation last layer on the electroosmotic flow. Experimental conditions: $(PDADMAC/PSS)_2$-$(Polycation)_1$ SMIL capillary coated, 40 cm total length capillary (30 cm to detector) × 50 µm i.d. BGE: 2 M acetic acid (pH 2.2). Hydrodynamic injection: 2.7 kPa, 4s. Co-injection of 0.002% DMF water (w/w). Protein mixture: (1) TI, (2) Myo, (3) RNAse A and (4) Lyz, at 0.25 gL^{-1} each in BGE. Temperature: 25°C. See Section 2.7 for the coating procedure.

Figure 5. Impact of PEGylation of the last PAH layer with 1kDa PEG (A) and 5kDa PEG (B). Same experimental conditions as in Figure 2. Reversed polarity was used for $(PDADMAC/PSS)_2$-$(PAH\text{-}g\text{-}(mPEG_{5kDa})_{0.11})_1$.

Figure 6. Impact of the PEGylation for the last PAH layer onMyo separation efficiency (A), Lyz separation efficiency (B) and peak resolution for the Myo / RNAse A pair (C). Same experimental conditions as in Figure 2. Reversed polarity was used for $(PDADMAC/PSS)_2$-$(PAH\text{-}g\text{-}(mPEG_{5kDa})_{0.11})_1$. See Figure SI 31 for impact on TI and RNAse A.

Figure 7. Evolution of shift frequency (continuous lines) and shift dissipation (dashed lines) for the 3rd harmonic during SMIL construction procedure in QCMD. Experimental conditions: see Figure 3. See detailed construction in supporting information Figure SI 32 to SI 34.

Table 1. Impact of the chemical nature of the last polycationic layer on protein retention factor (*k*) and on RSD on migration times at -10kV and -20kV. Experimental conditions: see Figure 2.

Table 2. Impact of last polycationic layer on SMIL construction and characteristics. Experimental conditions: see Figure 3.

Table 3. Impact of PEGylated polycation in the last layer on protein retention factor (*k*) and RSDt_m at -10kV and -20kV. Corresponding electropherograms and *H=f(u)* graphs are available in Supporting Information, from Figures SI 27 to Figure SI 30.

Table 4. Impact of the last polycationic layer on SMIL construction. Experimental conditions: see Figure 3.

Figures and Tables

Figure 1

Figure 2. Schematic representation of SMIL coatings used in this work based on $(PDADMAC/PSS)_2$ substructure. The last polycationic layer can be composed of unmodified PDADMAC, PAH, PEI, εPLL and αPLL, or their respective PEGylated chains with different chain lengths.

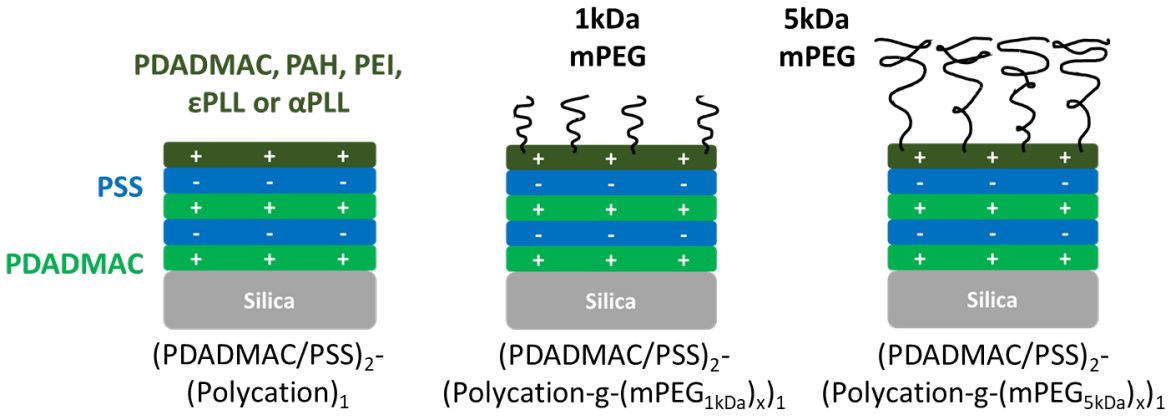

Figure 2

Figure 2. Impact of the nature of the last layer on protein separation at -10kV (A), on the *H*=f(*u*) curve in the case of Myo (B) and on the resolution of the Myo / RNAse A pair (C). Experimental conditions: $(PDADMAC/PSS)_2$-$(Polycation)_1$ SMIL coated capillary, 40 cm total length (30 cm to detector) × 50 µm i.d. BGE: 2 M acetic acid, pH 2.2. Hydrodynamic injection of proteins at 0.25 gL^{-1} each in BGE: 2.7 kPa, 4s (0.61% V_{tot}). Co-injection of 0.001% DMF in BGE (w/w): 2.7 kPa, 0.4s. Protein mixture: (1) TI, (2) Myo, (3) RNAse A and (4) Lyz. Applied voltages: -10kV, -12.5kV, -15kV, -17.5kV and -20kV. Temperature: 25°C. See Section 2.7 for the coating procedure.

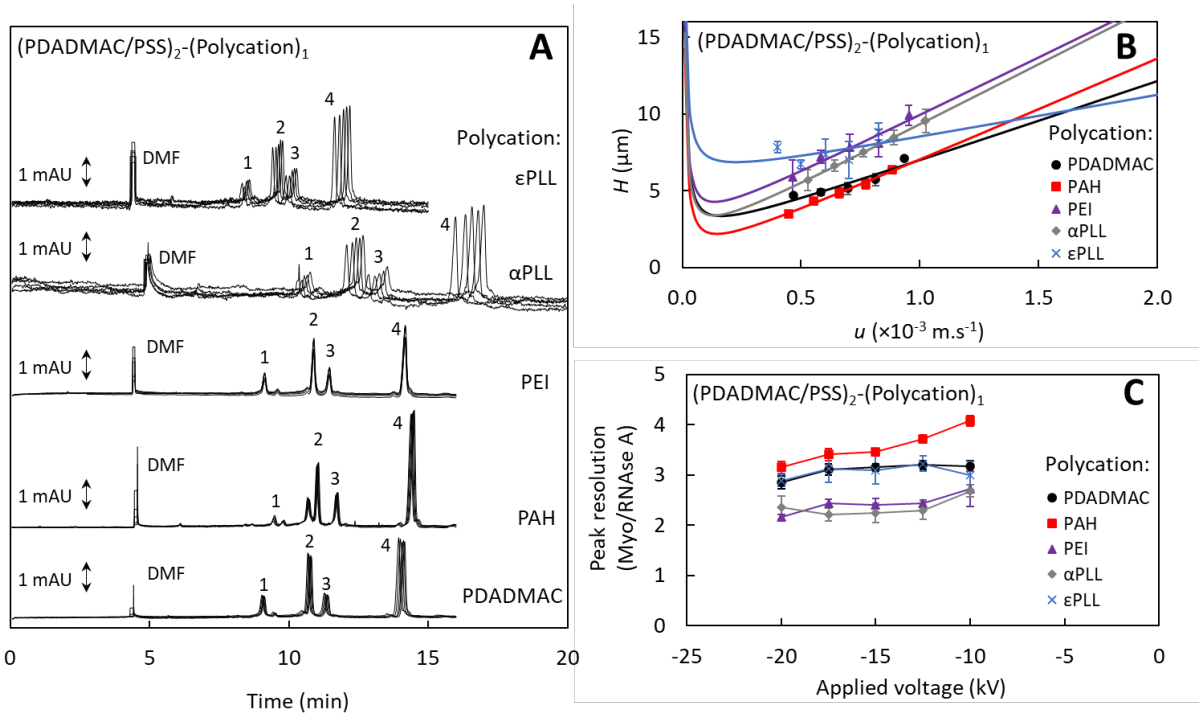

Figure 3

Figure 3. Evolution of frequency (continuous lines) and dissipation (dashed lines) shifts for the 3rd harmonic during SMIL construction procedure in QCMD. Experimental conditions: $(PDADMAC/PSS)_2$-$(Polycation)_1$ SMIL deposited on a silica-coated QCM sensor. Hydrodynamic flow: 0.05 $mLmin^{-1}$. Temperature: 23°C. Average $(PDADMAC/PSS)_2$ layers construction in grey. See Section 2.9 for the coating procedure.

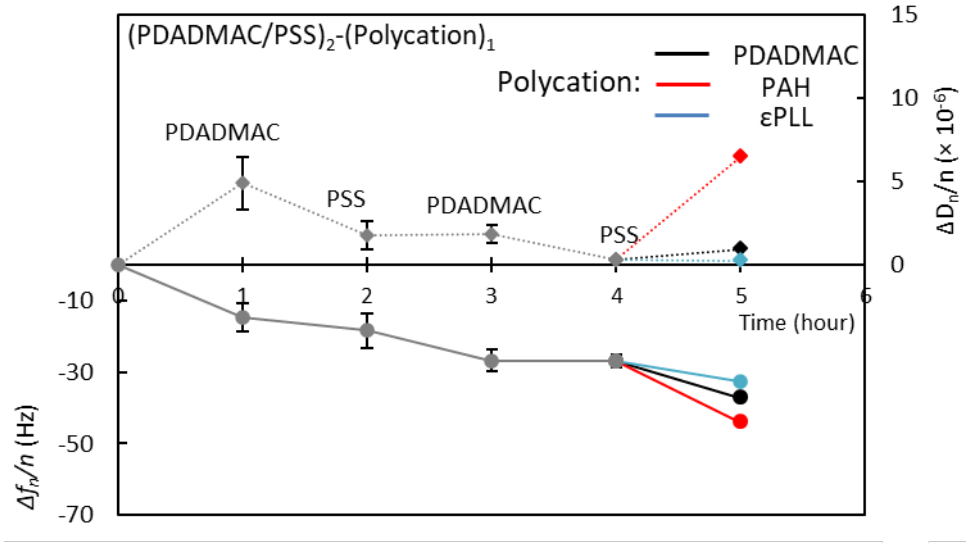

Figure 4

Figure 4. Impact of the PAH and PEI PEGylated polycation last layer on the electroosmotic flow. Experimental conditions: $(PDADMAC/PSS)_2$-(Polycation)$_1$ SMIL capillary coated, 40 cm total length capillary (30 cm to detector) × 50 µm i.d. BGE: 2 M acetic acid (pH 2.2). Hydrodynamic injection: 2.7 kPa, 4s. Co-injection of 0.002% DMF water (w/w). Protein mixture: (1) TI, (2) Myo, (3) RNAse A and (4) Lyz, at 0.25 gL^{-1} each in BGE. Temperature: 25°C. See Section 2.7 for the coating procedure.

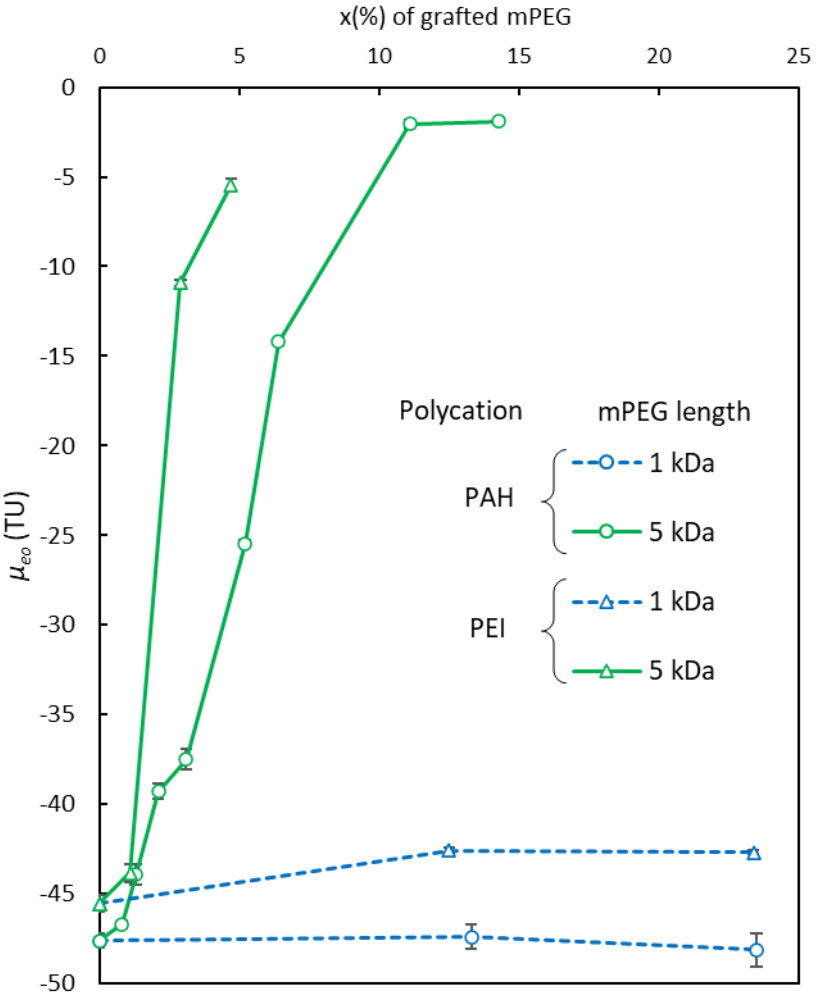

Figure 5

Figure 5. Impact of PEGylation of the last PAH layer with 1kDa PEG (A) and 5kDa PEG (B). Same experimental conditions as in Figure 2. Reversed polarity was used for $(PDADMAC/PSS)_2$-$(PAH\text{-}g\text{-}(mPEG_{5kDa})_{0.11})_1$.

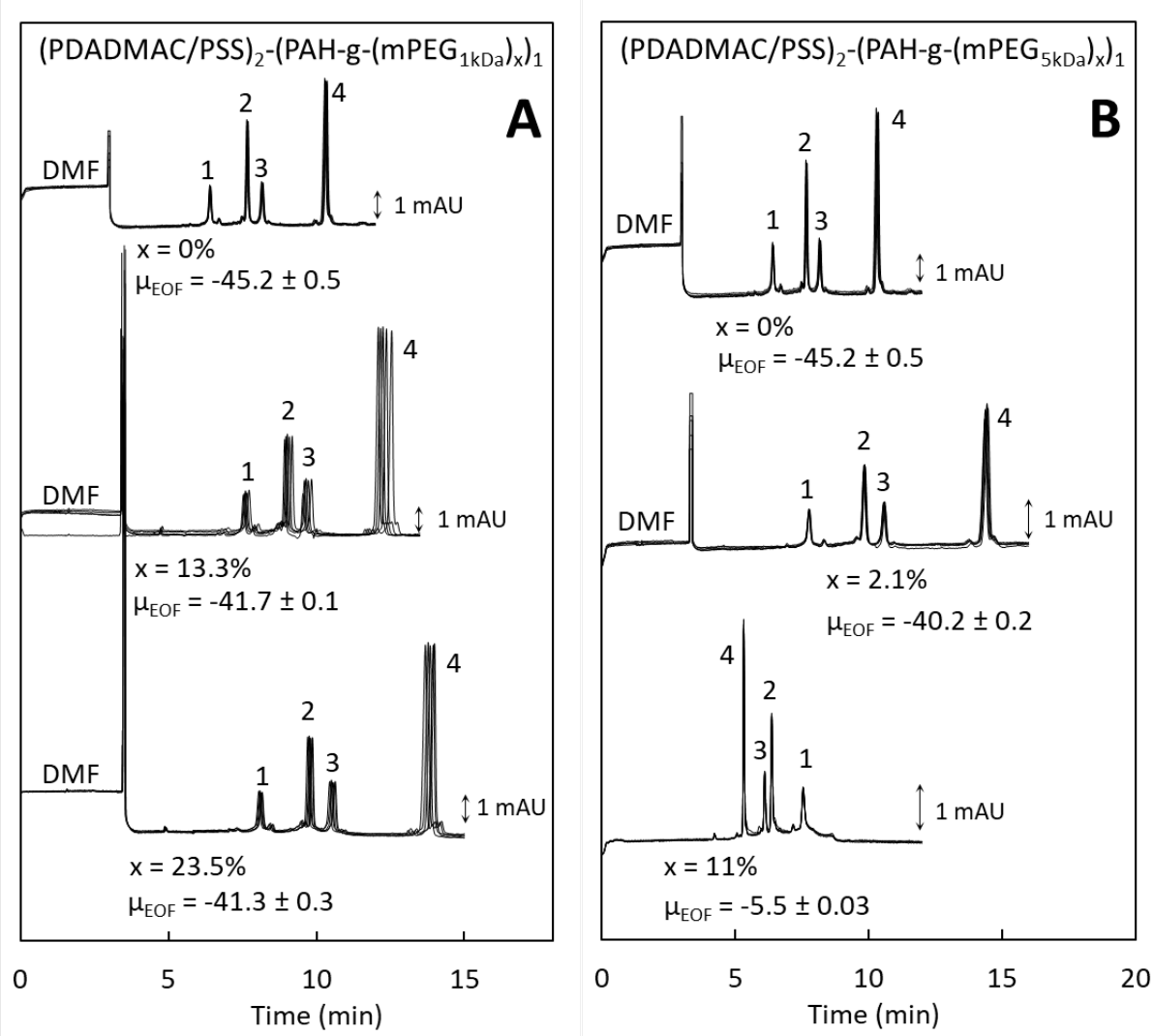

Figure 6

Figure 6. Impact of the PEGylation for the last PAH layer onMyo separation efficiency (A), Lyz separation efficiency (B) and peak resolution for the Myo / RNAse A pair (C). Same experimental conditions as in Figure 2. Reversed polarity was used for $(PDADMAC/PSS)_2$-$(PAH\text{-}g\text{-}(mPEG_{5kDa})_{0.11})_1$. See Figure SI 31 for impact on TI and RNAse A.

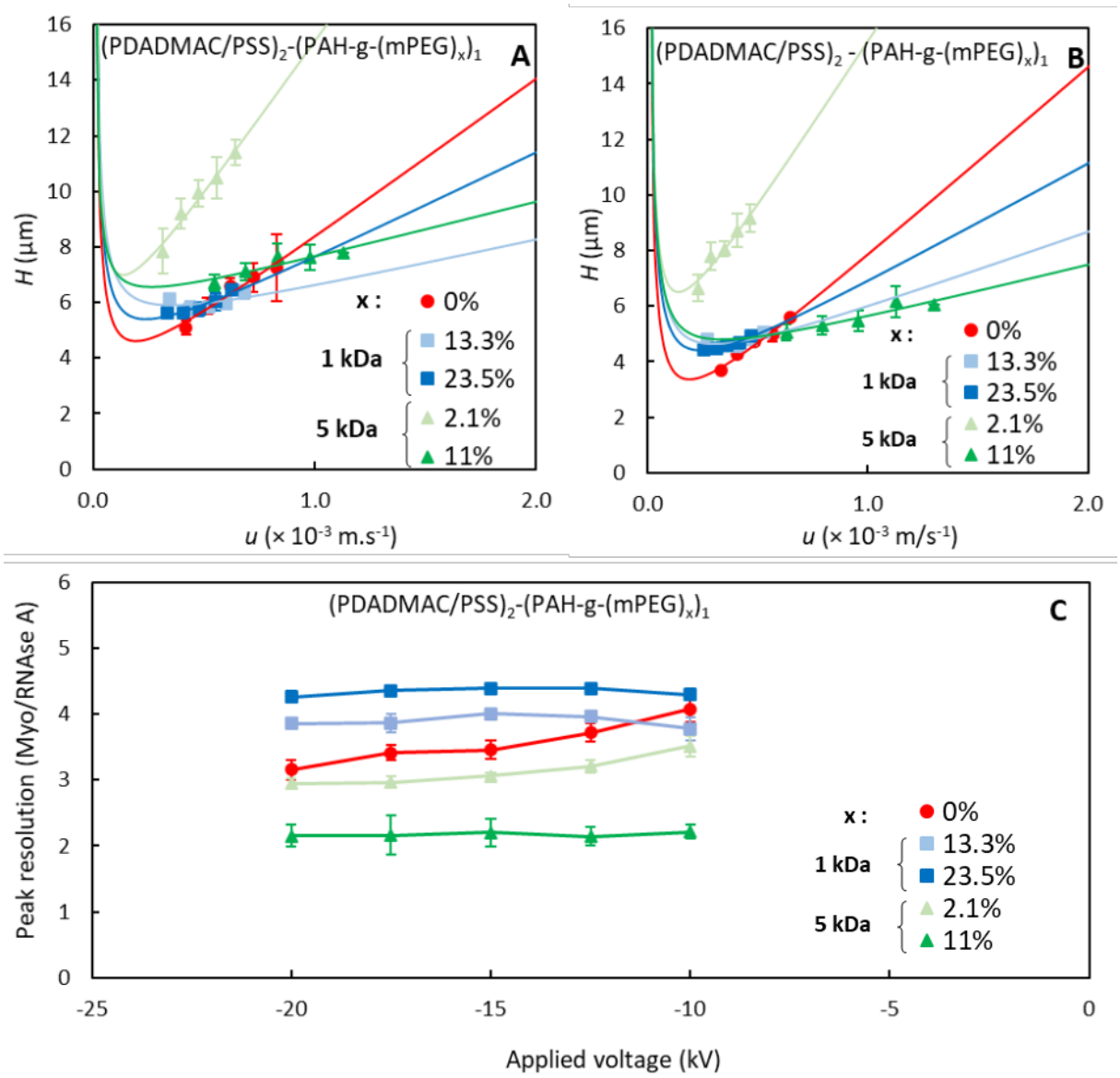

Figure 7

Figure 7. Evolution of shift frequency (continuous lines) and shift dissipation (dashed lines) for the 3rd harmonic during SMIL construction procedure in QCMD. Experimental conditions: see Figure 3. See detailed construction in supporting information Figure SI 32 to SI 34.

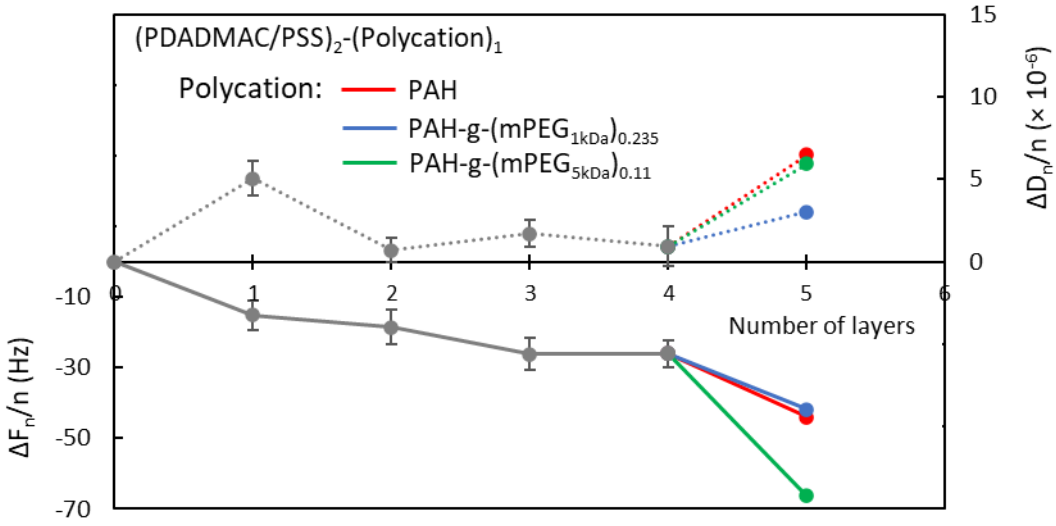

Table 1

Table 1. Impact of the chemical nature of the last polycationic layer on protein retention factor (*k*) and on RSD on migration times at -10kV and -20kV. Experimental conditions: see Figure 2.

Last layer polymer (μ_{eo})	Parameters	Proteins				
		TI	Myo	RNAse A	Lyz	Average
PDADMAC (-45.5 TU)	$k \times 10^{-2}$	6.8	5.1	6.8	7.3	6.5
	A [µm]	4.8	1.6	3.0	1.5	2.7
	RSDt_m (-10kV)	0.41	0.49	0.48	0.61	0.50
	RSDt_m (-20kV)	0.05	0.06	0.06	0.10	0.07
PAH (-45.2 TU)	$k \times 10^{-2}$	7.3	5.7	6.7	8.0	6.9
	A [µm]	4.3	0.3	2.4	0.7	1.9
	RSDt_m (-10kV)	0.34	0.41	0.44	0.54	0.43
	RSDt_m (-20kV)	0.06	0.05	0.10	0.15	0.09
PEI (-44.4 TU)	$k \times 10^{-2}$	8.3	6.2	7.2	7.6	7.3
	A [µm]	4.4	2.2	4.2	2.5	3.3
	RSDt_m (-10kV)	0.03	0.04	0.02	0.04	0.03
	RSDt_m (-20kV)	0.05	0.05	0.04	0.06	0.05
εPLL (-40.7 TU)	$k \times 10^{-2}$	3.1	3.7	4.6	3.9	3.8
	A [µm]	10.0	5.6	7.0	5.1	6.9
	RSDt_m (-10kV)	1.73	1.98	2.16	2.75	2.15
	RSDt_m (-20kV)	0.17	0.14	0.13	0.17	0.15
αPLL (-45.3 TU)	$k \times 10^{-2}$	8.7	6.3	7.3	7.9	7.5
	A [µm]	3.1	1.3	4.0	1.6	2.5
	RSDt_m (-10kV)	0.98	1.12	1.13	1.37	1.15
	RSDt_m (-20kV)	0.28	0.29	0.36	0.40	0.33

Table 2

Table 2. Impact of last polycationic layer on SMIL construction and characteristics. Experimental conditions: see Figure 3.

		Last layer		
	$(PDADMAC/PSS)_2$	PDADMAC	PAH	εPLL
Final $\Delta F_3/3$ shift [Hz]	-27	-37.2	-44	-32.5
Deposited areal mass [ng cm^{-1}]	478	599	779	575
SMIL thickness [nm]	4.5	6.8	7.6	6.6

Table 3

Table 3. Impact of PEGylated polycation in the last layer on protein retention factor (*k*) and RSDt_m at -10kV and -20kV. Corresponding electropherograms and *H=f(u)* graphs are available in Supporting Information, from Figures SI 27 to Figure SI 30.

	Last layer polymer (μ_{eo})	Parameters	Proteins				
			TI	Myo	RNAse A	Lyz	Average
1kDa	PAH (-45.2 TU)	$k \times 10^{-2}$	7.3	5.7	6.7	8.0	6.9
		A [µm]	4.3	0.3	2.4	0.7	1.9
		RSD_{tm} (-10kV)	0.34	0.41	0.44	0.54	0.43
		RSD_{tm} (-20kV)	0.06	0.05	0.10	0.15	0.09
	PAH 13.3% (-41.7 TU)	$k \times 10^{-2}$	5.8	3.0	3.7	5.1	4.4
		A [µm]	6.5	3.6	4.7	2.9	4.4
		RSD_{tm} (-10kV)	1.34	0.19	0.20	0.22	0.49
		RSD_{tm} (-20kV)	0.53	0.59	0.64	0.83	0.65
	PAH 23.5% (-41.3 TU)	$k \times 10^{-2}$	8.3	4.1	5.5	6.3	6.1
		A [µm]	4.5	2.6	3.6	2.3	3.3
		RSD_{tm} (-10kV)	1.36	1.54	1.62	2.03	1.64
		RSD_{tm} (-20kV)	0.41	0.46	0.48	0.61	0.49
5kDa	PAH 2.1% (-40.2 TU)	$k \times 10^{-2}$	9.4	7.8	9.5	10.8	9.4
		A [µm]	7.7	3.9	3.9	3.1	4.6
		RSD_{tm} (-10kV)	0.08	0.08	0.09	0.11	0.09
		RSD_{tm} (-20kV)	0.11	0.14	0.14	0.20	0.15
	PAH 11% (-5.5 TU)	$k \times 10^{-2}$	7.6	4.5	3.1	3.9	4.8
		A [µm]	8.3	3.8	5.5	3.5	5.3
		RSD_{tm} (-10kV)	0.02	0.02	0.01	0.02	0.02
		RSD_{tm} (-20kV)	0.04	0.05	0.05	0.01	0.04

Table 4

Table 4. Impact of the last polycationic layer on SMIL construction. Experimental conditions: see Figure 3.

		Last layer		
	$(PDADMAC/PSS)_2$	PAH	PAH-g-$(mPEG_{1kDa})_{0.235}$	PAH-g-$(mPEG_{5kDa})_{0.11}$
Final $\Delta F_n/n$ shift [Hz]	-26	-44	-41.9	-66.3
Deposited areal mass [ng cm^{-1}]	460.6	779	741	1174
SMIL thickness [nm]	4.3	7.6	7.2	11.4